Chinese Physics Letters

PAPER

Instability in Two-Sided Thermocapillary-Buoyancy Convection with Interfacial Phase Change*

To cite this article: Guo-Feng Xu *et al* 2020 *Chinese Phys. Lett.* **37** 014701

View the article online for updates and enhancements.

This content was downloaded from IP address 129.180.1.217 on 10/02/2020 at 09:30

CHIN. PHYS. LETT. Vol. 37, No. 1 (2020) 014701

Instability in Two-Sided Thermocapillary-Buoyancy Convection with Interfacial Phase Change *

Guo-Feng Xu(徐国峰)[1,2], Qiu-Sheng Liu(刘秋生)[1,2**], Jun Qin(秦军)[1,2], Zhi-Qiang Zhu(朱志强)[1]
[1] *Institute of Mechanics, Chinese Academy of Sciences, Beijing 100190*
[2] *University of Chinese Academy of Sciences, Beijing 100049*

(Received 14 August 2019)

A new model of two-phase thermocapillary-buoyancy convection with phase change at gas-liquid interface in an enclosed cavity subjected to a horizontal temperature gradient is proposed, rather than the previous one-sided model without phase change. We study the onset of multicellular convection and two modes of convective instability, and find four different flow regimes. Their transition map is compared with the non-phase-change condition. Our numerical results show the stabilizing effect of interfacial phase change on the thermocapillary-buoyancy convection.

PACS: 47.55.Ca, 47.55.dm, 47.20.Hw, 47.55.P– DOI: 10.1088/0256-307X/37/1/014701

Convective flow with a phase-change interface has recently gained a great deal of attention due to the great importance in scientific and industrial applications, such as crystal growth, two-phase capillary pumped loops and thermal management devices.[1–3] Both thermocapillary and buoyancy effects play a role in driving the convective flow in the liquid layer subjected to a horizontal temperature gradient along the free surface. The basic return-flow state becomes unstable when the temperature gradients exceed a critical value, and leads to steady cellular or oscillatory flow states. Combined phase-changed phenomena at gas-liquid interface, the onset of different flow states and convective instability become more complex due to the mass and heat transfer at the interface and the dynamic behaviors of vapor in the gas phase.

However, in most of the previous investigations on thermocapillary-buoyancy convection, interfacial phase-change effect is out of consideration. Using a linear stability analysis, Smith and Davis[4] found a new mode of instability in an infinite liquid layer bounded with horizontal temperature gradient when buoyancy effect is ignored, which is referred to as hydrothermal waves. They were then observed and confirmed in the experiment performed by Riley and Neitzel.[5] For a thin liquid layer ($O(1\,\text{mm})$) with a moderate Prandtl number $Pr = 13.9$, hydrothermal waves obliquely propagate from the cold to the hot end, whereas for a thicker liquid layer, a transition from the steady state to the oscillatory state with the increasing Marangoni number, instead of the hydrothermal waves, was found. Jiang *et al.*[6] and Wang *et al.*[7] investigated the instability of buoyancy-thermocapillary convection, but non-volatile liquids were employed in the experiments. Numerical simulation and theoretical analysis are essential to understand the mechanisms of onset of instability. However, for most previous studies,[8–11] phase change was ignored and the so-called “one-sided" model was employed.

We previously conducted an experiment with the volatile liquid in an open cavity differentially heated at the lateral walls, the average evaporating rate was measured and three major flow patterns were found when increasing the temperature difference.[12] Li *et al.*[13] found out that the onset of oscillating flow of a volatile liquid layer in a sealed cavity is greatly influenced by the concentration of noncondensables in the gas phase. One can find that interfacial phase-change effect and gas phase dynamics have great impacts on the onset of instability. Kazemi *et al.*[14] investigated the evaporation of water from a concave meniscus under a controlled pressure and temperature. Li *et al.*[15] employed the volatile liquid layer in a shallow annular pool to study the effect of surface evaporation on instability of thermocapillary-buoyancy convection, and found that the evaporation and buoyancy effects can suppress the flow destabilization when evaporation rate is low. Several numerical models[16,17] have taken into consideration of phase change, but the one-sided model was employed and the evaporation intensity is defined by an evaporation Biot number which was confined in the low temperature difference. Grigoriev and Qin[18] conducted a linear stability analysis on the two-phase convective flow and found that the effect of phase change and vapor transport in gas phase can significantly affect the stability of the flow. Qin *et al.*[19–21] performed 2D and 3D simulations using the two-sided model with phase change, but the dynamic Bond number for a single-component liquid layer is fixed at 0.853, which means that thermocapillary effect balances the buoyancy effect. Therefore, in the present study, we develop a numerical model accounting for interfacial phase change and dynamics of gas phase, and investigate the phase-change effect on the onset of instability of thermocapillary-buoyancy con-

*Supported by the National Natural Science Foundation of China (Grant Nos. 11532015 and U1738119), the China's Manned Space Program (TZ-1) and the Joint Project of CMSA-ESA Cooperation on Utilization in Space.
**Corresponding author. Email: liu@imech.ac.cn
© 2020 Chinese Physical Society and IOP Publishing Ltd

vection.

The two-sided model shown in Fig. 1 describes the thermocapillary-buoyancy convection in an enclosed cavity with phase change occurring at the liquid-gas interface. The incompressible, Newtonian liquid (volatile 0.65 cSt silicone oil) and gas (component of air and vapor, where air dominates) are contained in a two-dimensional rectangular cavity of height $H = H_\mathrm{l} + H_\mathrm{g}$ and width L, where the liquid layer aspect ratio $\Gamma = L/H_\mathrm{l}$ is 20, and the height ratio of gas layer to liquid layer, $\Pi = H_\mathrm{g}/H_\mathrm{l}$, is 3. Hereafter, subscripts l, g, v, a, i, c and h denote liquid phase, gas phase, vapor component, air component, liquid-gas interface, cold wall and hot wall, respectively. A temperature difference $\Delta T = T_\mathrm{h} - T_\mathrm{c}$ is imposed parallel to the free surface between the lateral walls.

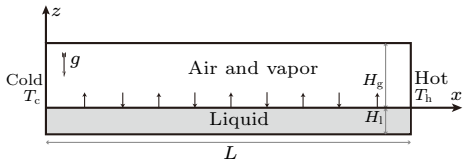

Fig. 1. Schematic of the two-sided model. White and grey regions correspond to the gas phase and liquid phase, respectively. Phase change (evaporation and condensation) occurs at the gas-liquid interface ($z = 0$) and the cavity is enclosed.

To reduce the number of parameters and make the mathematical model more concise, all the governing equations and boundary conditions are written in dimensionless form. In the liquid phase and gas phase, dimensionless Navier–Stokes equations with the Boussinesq approximation, heat transport equations and the advection-diffusion equation of vapor in gas phase are expressed as follows:

$$\nabla \cdot \boldsymbol{u}_\mathrm{l} = 0, \quad \nabla \cdot \boldsymbol{u}_\mathrm{g} = 0, \tag{1}$$

$$\begin{aligned} &\frac{\partial \boldsymbol{u}_\mathrm{l}}{\partial t} + \boldsymbol{u}_\mathrm{l} \cdot \nabla \boldsymbol{u}_\mathrm{l} = -\nabla p_\mathrm{l} + \nabla^2 \boldsymbol{u}_\mathrm{l} + \frac{Ra}{Pr}\Theta_\mathrm{l}\boldsymbol{k}, \\ &\frac{\partial \boldsymbol{u}_\mathrm{g}}{\partial t} + \boldsymbol{u}_\mathrm{g} \cdot \nabla \boldsymbol{u}_\mathrm{g} = -\frac{1}{\rho^*}\nabla p_\mathrm{g} + \nu^* \nabla^2 \boldsymbol{u}_\mathrm{g} + \frac{Ra}{Pr}\beta^* \Theta_\mathrm{g}\boldsymbol{k}, \end{aligned} \tag{2}$$

$$\frac{\partial \Theta_\mathrm{l}}{\partial t} + \boldsymbol{u}_\mathrm{l} \cdot \nabla \Theta_\mathrm{l} = \frac{1}{Pr}\nabla^2 \Theta_\mathrm{l},$$

$$\frac{\partial \Theta_\mathrm{g}}{\partial t} + \boldsymbol{u}_\mathrm{g} \cdot \nabla \Theta_\mathrm{g} = \frac{\alpha^*}{Pr}\nabla^2 \Theta_\mathrm{g}, \tag{3}$$

$$\frac{\partial Y_\mathrm{v}}{\partial t} + \boldsymbol{u}_\mathrm{g} \cdot \nabla Y_\mathrm{v} = \frac{\nu^*}{Sc}\nabla^2 Y_\mathrm{v}, \tag{4}$$

where $\boldsymbol{u}$, p, $\Theta = (T - T_\mathrm{c})/\Delta T$ and $Y_\mathrm{v} = \rho_\mathrm{v}/\rho_\mathrm{g}$ represent the dimensionless velocity vector, pressure, temperature and the mass fraction of vapor, respectively. Properties of the working liquid (0.65 cSt silicone oil) are the density $\rho = 761\,\mathrm{kg/m^3}$, the thermal diffusivity $\alpha = 9.52 \times 10^{-8}\,\mathrm{m^2/s}$, the thermal conductivity $k = 0.1\,\mathrm{W/(m{\cdot}K)}$, the thermal expansion coefficient $\beta = 1.34 \times 10^{-3}/\mathrm{K}$, the kinematic viscosity $\nu = 6.5 \times 10^{-7}\,\mathrm{m^2/s}$ and the dynamic viscosity $\mu = 4.95 \times 10^{-4}\,\mathrm{kg/(m{\cdot}s)}$; $\boldsymbol{k}$ is the unit vector in the z direction and superscript * denotes the ratio of the physical parameters of the gas to the liquid. $Pr = \nu_\mathrm{l}/\alpha_\mathrm{l} = 6.83$ is the Prandtl number, $Ra = g\beta_l \Delta T H_\mathrm{l}^3/(\nu_\mathrm{l}\alpha_\mathrm{l})$ is the Rayleigh number, and $Sc = \nu_\mathrm{g}/D = 0.604$ is the Schmidt number. $D = 2.5 \times 10^{-5}\,\mathrm{m^2/s}$ is the diffusion coefficient of the vapor in air. We use H_l, $H_\mathrm{l}^2/\nu_\mathrm{l}$, $\nu_\mathrm{l}/H_\mathrm{l}$, $\rho_\mathrm{l}\nu_\mathrm{l}^2/H_\mathrm{l}^2$ and ΔT as scales for length, time, velocity, pressure and temperature, respectively.

For 0.65 cSt silicone oil, the surface-tension number $S = \rho_\mathrm{l} H_\mathrm{l} \sigma_\mathrm{l}/\mu_\mathrm{l}^2$ tends to infinity and the capillary number $\mathrm{Ca} = \mu_\mathrm{l} u_\mathrm{l}/\sigma_\mathrm{l}$ tends to zero, thus the liquid-gas interface is assumed to be flat and non-deformable. The surface tension at the interface is considered to be a linear function of temperature: $\sigma = \sigma_0 - \sigma_T(T - T_0)$, where $\sigma_0 = 1.59 \times 10^{-2}\,\mathrm{N/m}$ is the surface tension at the reference temperature $T_0 = T_\mathrm{c}$ and $\sigma_T = -\partial\sigma/\partial T = 7 \times 10^{-5}\,\mathrm{N/(m{\cdot}K)}$ is the surface tension coefficient, which is constant and positive. At the interface, no-slip condition for horizontal velocity in each phase is

$$u_\mathrm{l} = u_\mathrm{g}, \tag{5}$$

and tangential stress balance between shear stress and thermocapillary stress is given by

$$\left(\frac{\partial u_\mathrm{l}}{\partial z} + \frac{\partial v_\mathrm{l}}{\partial x}\right) - \mu^* \left(\frac{\partial u_\mathrm{g}}{\partial z} + \frac{\partial v_\mathrm{g}}{\partial x}\right) = -\frac{Ma}{Pr}\frac{\partial \Theta_\mathrm{i}}{\partial x}, \tag{6}$$

where $Ma = \sigma_T \Delta T H_\mathrm{l}/(\mu_\mathrm{l}\alpha_\mathrm{l})$ is the Marangoni number. Scaling the interfacial phase-change mass flux j with $k_\mathrm{l}\Delta T/(H_\mathrm{l}\mathcal{L})$, where $\mathcal{L} = 2.14 \times 10^5\,\mathrm{J/kg}$ is the latent heat. Introducing the dimensionless evaporation number $E = k_\mathrm{l}\Delta T/(\rho_\mathrm{l}\nu_\mathrm{l}\mathcal{L})$, which indicates the ratio of phase-change rate to viscous diffusion rate, we obtain the interfacial mass conservation and mass flux balance in the presence of rate-limiting phase-change process as follows:

$$\begin{aligned} Ej &= v_\mathrm{l} = \rho^* v_\mathrm{g}, \\ Ej &= -\frac{\rho^*\nu^*}{Sc\,(1 - Y_\mathrm{v})}\frac{\partial Y_\mathrm{v}}{\partial z}. \end{aligned} \tag{7}$$

The classic Hertz–Knudsen equation based on the kinetic theory is used to describe the non-equilibrium conditions for interfacial dimensional phase-change mass flux

$$j_m = \frac{2\lambda}{2 - \lambda}\sqrt{\frac{M_\mathrm{v}}{2\pi\bar{R}}}\left(\frac{p_\mathrm{sat}\,(\Theta_\mathrm{i})}{\sqrt{T_\mathrm{i}}} - \frac{p_\mathrm{v}\,(Y_\mathrm{v})}{\sqrt{T_\mathrm{g}}}\right), \tag{8}$$

where $\lambda = 1$ is the accommodation coefficient, M_v is the molecular weight of the vapor, and $\bar{R} = 8.314\,\mathrm{J/(mol{\cdot}K)}$ is the universal gas constant. Here $p_\mathrm{sat}(\Theta_\mathrm{i})$ is the dimensional interfacial saturation vapor pressure which can be computed using the Clausius-Clapeyron relation

$$p_\mathrm{sat}\,(\Theta_\mathrm{i}) = p_{\mathrm{v},0}\exp\left[-\frac{M_\mathrm{v}\mathcal{L}}{\bar{R}}\left(\frac{1}{T_\mathrm{i}} - \frac{1}{T_0}\right)\right], \tag{9}$$

where $p_{\mathrm{v},0} = 4400\,\mathrm{Pa}$ is the dimensional saturation vapor pressure at the reference temperature $T_0 = 293.15\,\mathrm{K}$. The gas phase is a mixture of air and vapor, and each component is considered to be ideal gas,

according to the Dalton law of partial pressures, the dimensional vapor pressure $p_{\rm v}(Y_{\rm v})$ is given by

$$p_{\rm v}\left(Y_{\rm v}\right)=p_{\rm g}\frac{Y_{\rm v}}{Y_{\rm v}+r\left(1-Y_{\rm v}\right)}, \tag{10}$$

where $r=M_{\rm v}/M_{\rm a}=5.6$ is the molecular weight ratio of vapor to air. Particularly, $p_{\rm sat}(\Theta_{\rm i})$ and $p_{\rm v}(Y_{\rm v})$ are scaled by $p_{\rm g}$, Eq. (8) can be transformed into the dimensionless form

$$QEj=\frac{p_{\rm v,0}}{p_{\rm g}}\exp\left[-\frac{M_{\rm v}\mathcal{L}}{\bar{R}}\left(\frac{1}{T_{\rm i}}-\frac{1}{T_0}\right)\right]-\frac{Y_{\rm v}}{Y_{\rm v}+r\left(1-Y_{\rm v}\right)}, \tag{11}$$

Q is a dimensionless number that indicates the resistance to phase change caused by interfacial non-equilibrium effect and defined as

$$Q=\frac{(2-\lambda)\,\rho_{\rm l}\nu_{\rm l}}{2\lambda p_{\rm g}H_{\rm l}}\sqrt{\frac{2\pi\overline{R}T_{\rm i}}{M_{\rm v}}}. \tag{12}$$

The temperature at the interface is considered to be continuous,

$$\Theta_{\rm l}=\Theta_{\rm g}=\Theta_{\rm i}. \tag{13}$$

However, the heat flux is discontinuous due to the latent heat absorbed in liquid evaporation and released in vapor condensation, the energy balance gives

$$j=-\frac{\partial\Theta_{\rm l}}{\partial z}+k^{*}\frac{\partial\Theta_{\rm g}}{\partial z}. \tag{14}$$

The remaining boundary conditions at all the walls are standard no-slip and no-penetration conditions expressed in the following.

At the top adiabatic wall ($z=3$),

$$u_{\rm g}=v_{\rm g}=0,\quad \frac{\partial\Theta_{\rm g}}{\partial z}=0,\quad \frac{\partial Y_{\rm v}}{\partial z}=0. \tag{15}$$

At the bottom adiabatic wall ($z=-1$),

$$u_{\rm l}=v_{\rm l}=0,\quad \frac{\partial\Theta_{\rm l}}{\partial z}=0. \tag{16}$$

At the left cold wall ($x=0$),

$$\Theta_{\rm l}=\Theta_{\rm g}=0,\ u_{\rm l}=v_{\rm l}=u_{\rm g}=v_{\rm g}=0,\ \frac{\partial Y_{\rm v}}{\partial x}=0. \tag{17}$$

At the right hot wall ($x=20$),

$$\Theta_{\rm l}=\Theta_{\rm g}=1,\ u_{\rm l}=v_{\rm l}=u_{\rm g}=v_{\rm g}=0,\ \frac{\partial Y_{\rm v}}{\partial x}=0. \tag{18}$$

The governing equations in both liquid and gas phases along with the boundary conditions are solved based on the finite difference method. Fully second order accurate projection method is used to decouple the computation of pressure from velocity in the Navier–Stokes equations, leading to a pressure Poisson equation at each time step which is solved by Fourier analysis-cyclic reduction algorithm (FACR). The diffusion terms are discretized by the Crank–Nicolson scheme, the convective terms are discretized by the Adams–Bashforth scheme and all the spatial derivatives are discretized by standard central finite difference. Uniform staggered mesh $800\times(40+120)$ is selected for good grid convergence. The accuracy of the two-sided model is validated by comparing the two-layer flow without phase change given by Liu *et al.*,[22] two-phase flow with phase change given by Qin *et al.*,[19] and the experimental results of the evaporating liquid layer given by Zhu and Liu.[12]

We introduce the laboratory Marangoni number to compare our numerical results with other experimental studies, which applies the imposed horizontal temperature gradient $\Delta T/L$,

$$Ma_{\rm L}=\frac{\sigma_T H_{\rm l}^2}{\mu_{\rm l}\alpha_{\rm l}}\frac{\Delta T}{L}=\frac{Ma}{\Gamma}, \tag{19}$$

and the interfacial effective Marangoni number which applies the practical temperature gradient in the core region of the interface $\tau=\partial T_{\rm i}/\partial x$,

$$Ma_{\rm i}=\frac{\sigma_T H_{\rm l}^2\tau}{\mu_{\rm l}\alpha_{\rm l}}. \tag{20}$$

The strength of buoyancy convection and thermocapillary convection is characterized by the Rayleigh number and Marangoni number, respectively. To measure the relative strength of buoyancy force to thermocapillary force, one should introduce the dynamic Bond number as

$$\mathrm{Bo}=\frac{Ra}{Ma}=\frac{\rho_{\rm l}g\beta_{\rm l}H_{\rm l}^2}{\sigma_T}, \tag{21}$$

which only depends on the height of the liquid layer.

Four major flow regimes are found in the thermocapillary-buoyancy convection of the volatile liquid layer in an enclosed cavity, followed by Riley and Neitzel,[5] these different flow regimes are referred to as steady unicellular flow (SUF), steady multicellular convection (SMC), oscillating multicellular convection (OMC) and hydrothermal waves (HTW). The typical flow patterns are shown in Fig. 2. Subjected to the imposed horizontal temperature gradient, fluids in both liquid phase and gas phase flow counterclockwise and clockwise, respectively, which are driven by thermocapillary force on the interface and buoyancy force in the bulk. When $Ma_{\rm L}$ is small, only one uniform convection cell is observed in the core region of the steady flow away from the lateral walls. As $Ma_{\rm L}$ is increased, separate small rolls start to emerge from the hot side to the cold side in sequence until several uniform and steady rolls occupy the core region. The onset of the time-dependent flow, which propagates from the cold side to the hot side in travelling-wave state (HTW when $\mathrm{Bo}<0.22$) or oscillates in standing-wave state (OMC when $\mathrm{Bo}>0.22$) depending on the dynamic Bond number, shows up when $Ma_{\rm L}$ exceeds the critical value. Time evolutions of the typical periodic oscillating multicellular convection are shown in

Fig. 3 and the dimensionless fundamental frequency for oscillating flow is $f_1 = 2.78$.

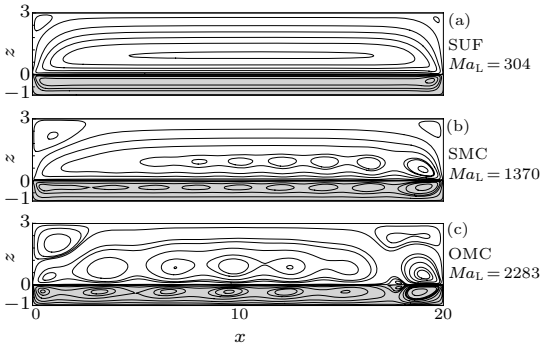

Fig. 2. Streamlines of steady unicellular flow (SUF), steady multicellular convection (SMC) and one typical instant of time during the oscillation period of oscillating multicellular convection (OMC) when Bo = 0.6.

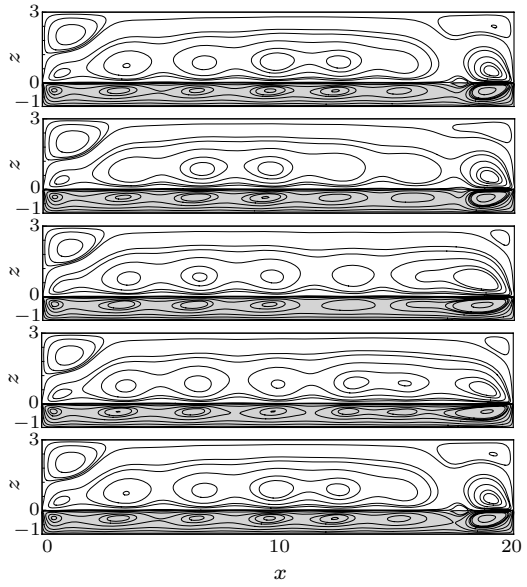

Fig. 3. Time evolution of the streamlines at five evenly spaced instants over one oscillating period for oscillating multicellular convection for $Ma_L = 2283$ and Bo = 0.6.

The transition map of different flow regimes is illustrated in Fig. 4. To investigate the impact of phase change on convection instability, the corresponding cases without phase change ($j = 0$ on the interface and $Y_v = 0$ in gas phase) are compared numerically and experimentally, respectively. As Bo increases, the critical Ma_L for the onset of the instability also increases due to the stabilizing effect of the increasing buoyancy force. In our numerical simulation and in comparison with the previous experimental results given in Refs. [5,8], it is also found that the critical Ma_L of the onset of the time-dependent flow for phase-change model is obviously higher than that of the model omitting phase change.

Due to the evaporation (distributed at the hot side) and condensation (distributed at the cold side) occurs at the interface, the latent heat absorbed and released, respectively, can decrease the average interfacial temperature gradient along the gas-liquid interface (shown in Fig. 5), which determines the strength of the thermocapillary effect on the thermal convection. Thus, the critical Ma_L for the onset of the instability increases as a result of phase change at the interface.

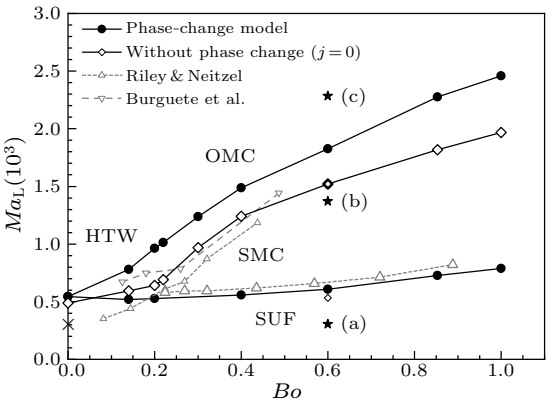

Fig. 4. Transition map of flow regimes from steady unicellular flow (SUF) to hydrothermal waves (HTW), steady multicellular convection (SMC) and oscillating multicellular convection (OMC) for models with and without phase change ($j = 0$). The points noted by symbols ⋆(a), ⋆(b) and ⋆(c) correspond respectively to three typical flow patterns shown in Fig. 2.

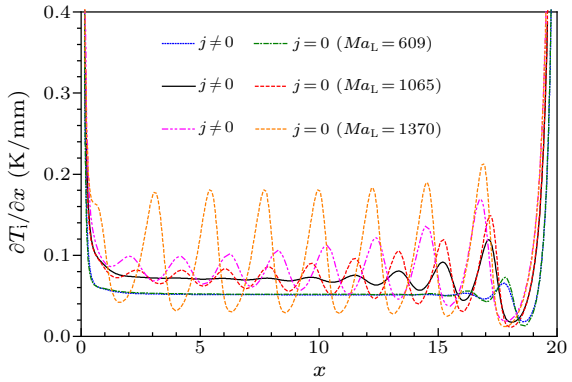

Fig. 5. Interfacial temperature gradient $\tau = \partial T_i/\partial x$ for two-phase flow with phase change ($j \neq 0$) and without phase change ($j = 0$) when Bo = 0.6.

The numerical results are also compared with the experimental data reported by Riley and Neitzel[5] and Burguete *et al.*[8] These two experiments are in a large spanwise aspect ratio which allows the 2D approximation in the streamwise direction. The critical Ma_L for the transition from SUF to SMC of the phase-change model are in good agreement with Riley and Neitzel, even omitting phase change, the critical Ma_L are very close to the phase-change model. This phenomenon can be elucidated by interfacial temperature gradient τ, as shown in Fig. 5. At relatively low Ma_L, convection is within the SUF regime, phase-change effect is relatively weak and unable to alter the interfacial temperature gradient in the core region and then the flow regime almost remains unchanged. As Ma_L is increased, the average value and fluctuation amplitude of τ is apparently reduced under the influence of in-

tensive phase-change effect. It is notable that phase change has a minor influence on the thermal boundary layer near the lateral walls.

Also shown in Fig. 4, specially for microgravity condition (Bo = 0) in space where buoyancy convection vanishes, the critical $\mathrm{Ma_i}$ for the onset of HTW predicted by Smith and Davis[4] is approximately equal to 260, which is very close to our numerical result $\mathrm{Ma_i} = 280$ for the non-phase-change condition, but lower than the critical $Ma_\mathrm{i} = 311$ for phase-change condition. In fact, Burguete *et al.*[8] also used a volatile 0.65 cSt Rhône-Poulenc silicone oil as the working liquid whose $Pr = 10.3$ is slightly larger than ours, but special treatment of liquid was applied to reduce evaporation in their experiment. Thus, the critical Ma_L of our numerical simulation for none phase-change condition agrees well with Burguete's experiment for the onset of instability within the range of $0.14 \leq \mathrm{Bo} \leq 0.4$.

In summary, a two-sided model of thermocapillary-buoyancy convection, which fully accounts for the interfacial phase-change heat transfer and the gas flow, is proposed and analyzed numerically. A new feature of instability and flow regime transition of the flow coupling with phase-change effect on the interface are found and the mechanism of interfacial phase-change effect is analyzed numerically. The critical Ma_L of phase-changed thermocapillary-buoyancy convection for onset of steady multicellular convection and the instability transition is also compared with the experimental results. In this study, it is found obviously that the phase change of evaporation and condensation plays an evident role of stabilizing the thermocapillary convection due to the decrease of the interfacial temperature gradient and thermocapillary force at interface. In other words, the mass and heat transfer with phase change at gas-liquid interface tends to stabilize the thermocapillary-buoyancy flows.

References

[1] Li Y R, Zhang L, Zhang L and Yu J J 2018 *Int. J. Thermal Sci.* **130** 168
[2] Chen P C and Lin W K 2001 *Appl. Therm. Eng.* **21** 1739
[3] Abe Y, Iwaski A and Tanaka K 2005 *Microgravity Sci. Technol.* **16** 148
[4] Smith M K and Davis S H 1983 *J. Fluid Mech.* **132** 119
[5] Riley R J and Neitzel G P 1998 *J. Fluid Mech.* **359** 143
[6] Jiang H, Duan L and Kang Q 2017 *Chin. Phys. B* **26** 114703
[7] Wang J, Duan L and Kang Q 2017 *Chin. Phys. Lett.* **34** 074703
[8] Burguete J, Mukolobwiez N, Daviaud F, Garnier N and Chiffaudel A 2001 *Phys. Fluids* **13** 2773
[9] Shevtsova V M, Nepomnyashchy A A and Legros J C 2003 *Phys. Rev. E* **67** 066308
[10] Zhou X M and Huang H L 2012 *Chin. Phys. Lett.* **29** 074704
[11] Li Y R, Zhang S and Zhang L 2019 *Int. J. Thermal Sci.* **145** 105983
[12] Zhu Z Q and Liu Q S 2010 *Chin. Sci. Bull.* **55** 233
[13] Li Y, Grigoriev R and Yoda M 2014 *Phys. Fluids* **26** 122112
[14] Kazemi M A, Nobes D S and Elliott J A W 2017 *Langmuir* **33** 4578
[15] Li J J, Zhang L, Zhang L, Li Y R and Quan X J 2019 *Int. J. Heat Mass Transfer* **140** 828
[16] Liu R, Liu Q S and Hu W R 2005 *Chin. Phys. Lett.* **22** 402
[17] Ji Y, Liu Q S and Liu R 2008 *Chin. Phys. Lett.* **25** 608
[18] Grigoriev R O and Qin T 2018 *J. Fluid Mech.* **838** 248
[19] Qin T, Tuković Ž and Grigoriev R O 2014 *Int. J. Heat Mass Transfer* **75** 284
[20] Qin T, Tuković Ž and Grigoriev R O 2015 *Int. J. Heat Mass Transfer* **80** 38
[21] Qin T and Grigoriev R O 2018 *Int. J. Heat Mass Transfer* **127** 308
[22] Liu Q S, Chen G and Roux B 1993 *Int. J. Heat Mass Transfer* **36** 101